Note on Earhtquake Seismology <3> Friction and rupture growth

Hideo Aochi

1. Quantitaive Framework
2. Crack theory and fracture
3. Friction and rupture growth
4. Numerical model
5. Earthquake scaling
6. Obsevational seismology

15 December 2025

Friction = Constitutive relation

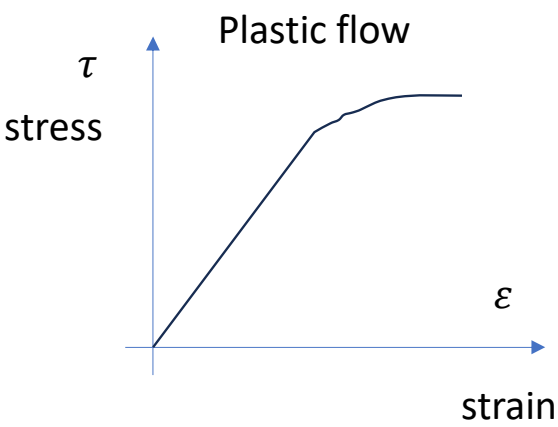

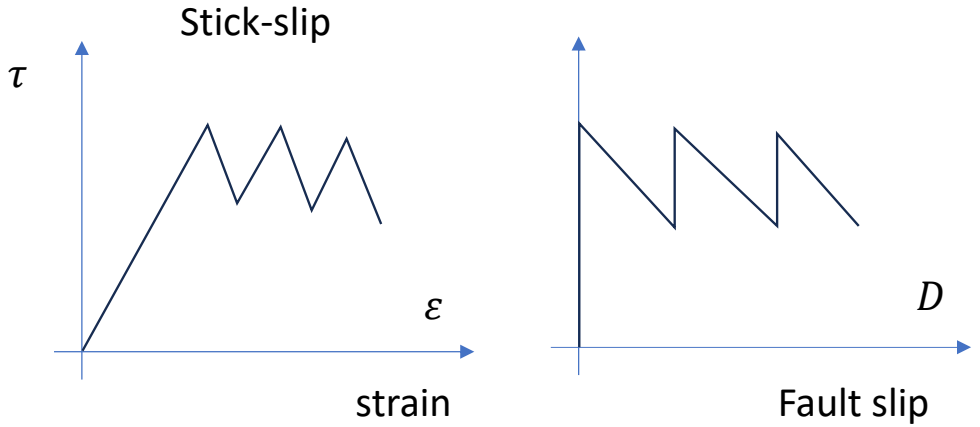

$$\dot{\varepsilon} = Af(\sigma)\exp\left(-\frac{Q}{RT}\right)$$

$$f(\sigma) = \sigma^n; n > 1$$

creep

$$\tau = \tau\left(D, \dot{D}\right) = \tau\left(D, \dot{D}; \sigma_n^{eff}, T, \dots\right)$$

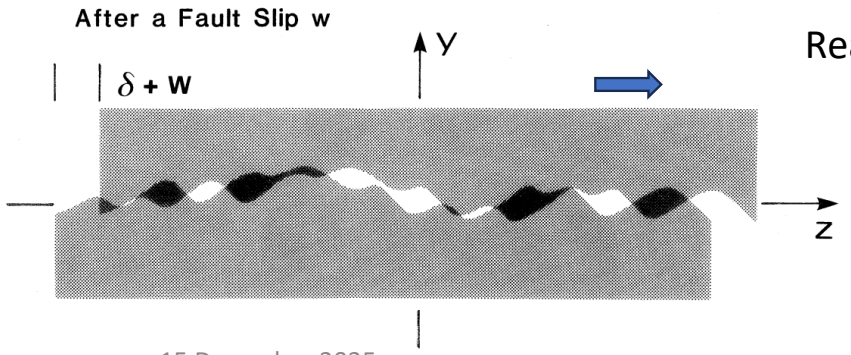

Real contact area S

$$F = A \cdot S$$

$$S \propto N$$

Rock experiments

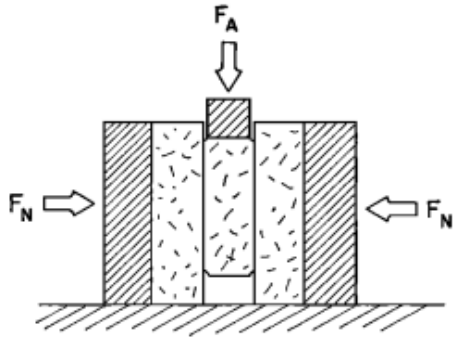

Fig. 1. Schematic diagram of apparatus.

Dieterch (1972): 6 x 6 x 1.5 cm

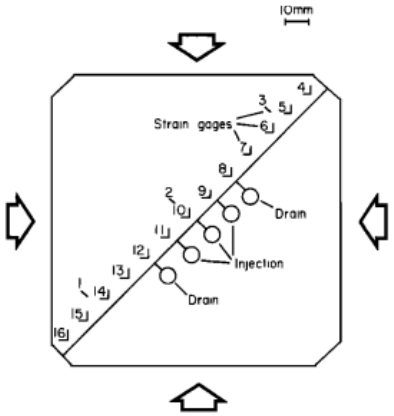

Fig. 1. Sample configuration showing locations of strain gages. Gages 1–3 give normal strains, and gages 4–16 give shear strains parallel to the fault.

Dietrich (1978): 12.7 x 12.7 x 4 cm

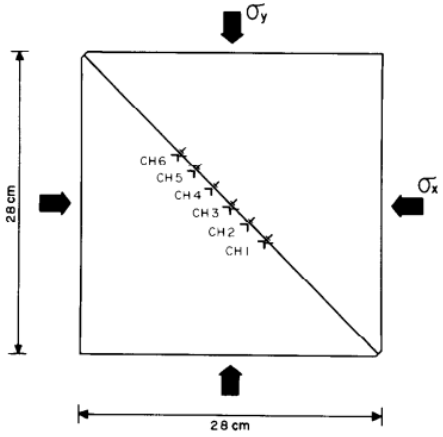

Fig. 1. Sample configuration with strain gage sensors in position.

Ohnaka et al. (1987)

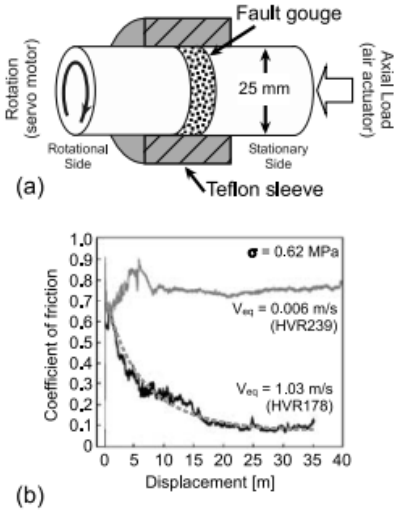

Mizoguchi et al. (2007)

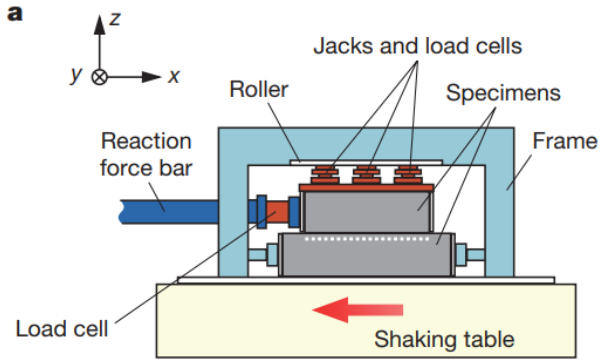

Yamashita et al. (2015): 1.5 m length

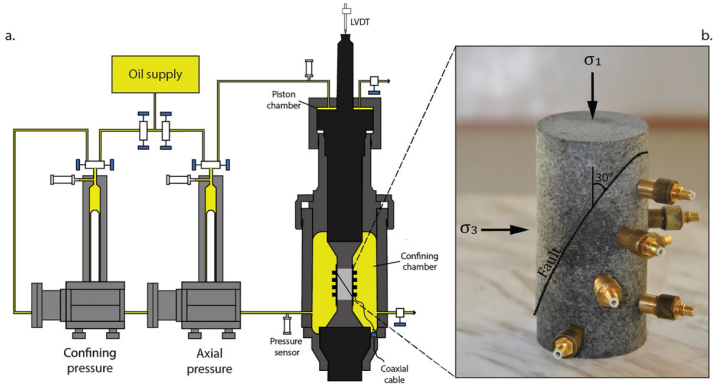

Marty et al. (2023): 88mm long

Rupture nucleation and propagation

Dieterich (1978)

Preseismic Fault Slip and Earthquake Prediction

J. H. DIETERICH

U.S. Geological Survey, Menlo Park, California 94025

It is proposed that preseismic fault creep may be the underlying process that is responsible for observations of earthquake precursors. The assertion that fault creep precedes earthquakes is supported by evidence from at least some earthquakes and by analogy with detailed laboratory observations. Laboratory observations of stick slip reveal that at least two stages of preseismic slip are an intrinsic part of the process leading to seismic slip on preexisting faults with inhomogeneous stress or strength. During the slowly propagating first stage of creep it is assumed that the length of the creeping fault segment is proportional to the source length of the subsequent earthquake. The data giving the well-known relationship between precursor time and earthquake magnitude are closely satisfied if the rate of propagation of the first stage of creep is independent of fault length. Long-term precursors may arise because of stress-strain variations during the first stage of fault creep. Observations of short-term precursors immediately prior to earthquakes may be related to the second short-lived state of preseismic fault slip seen in stick slip experiments.

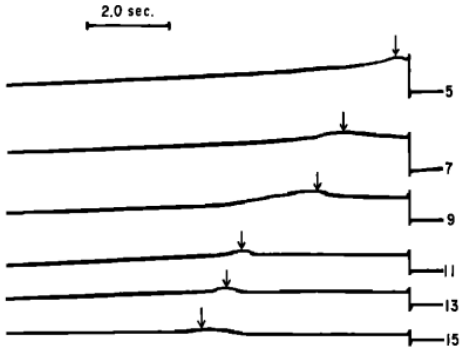

Fig. 2. Slow-speed oscillograph record of stick-slip event showing large amounts of slowly propagating preseismic slip. Numbers refer to gage locations. Arrows mark the time at which fault slip began at each strain gage.

Ohnaka et al. (1987)

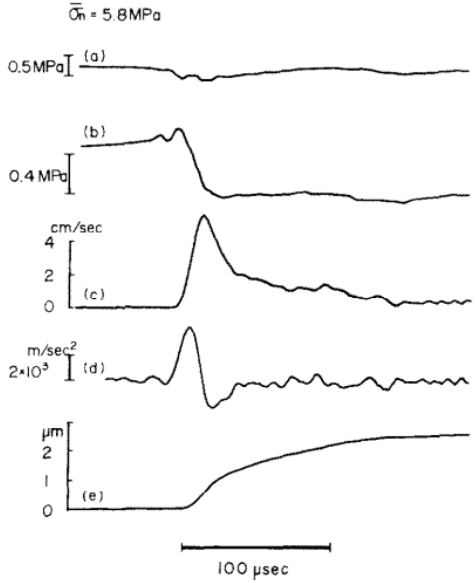

Fig. 4. An example of recorded signals at a location along the fault in sample A during a stick-slip shear failure generated at an average local normal stress of 5.80 MPa: (a) dynamic normal stress, (b) dynamic shear stress, (c) slip velocity, (d) slip acceleration and (e) relative displacement. The slip velocity and acceleration are the time derivatives of the displacement and the slip velocity, respectively.

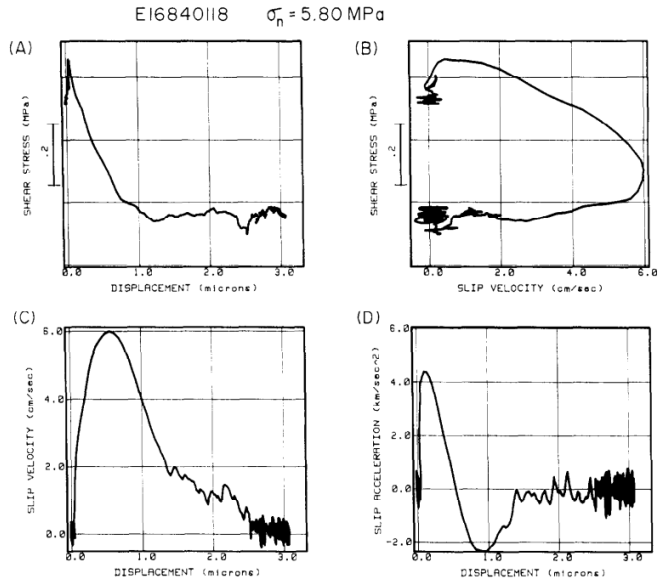

ts of (A) the shear stress against the displacement, (B) the shear stress against the slip velocity, (C) the slip velocity against cement, and (D) the slip acceleration against the displacement for the data shown in Fig. 4.

A Model of Breakdown Zon

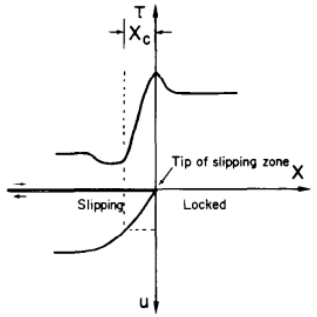

Rupture nucleation and propagation

Yamashita et al. (2021)

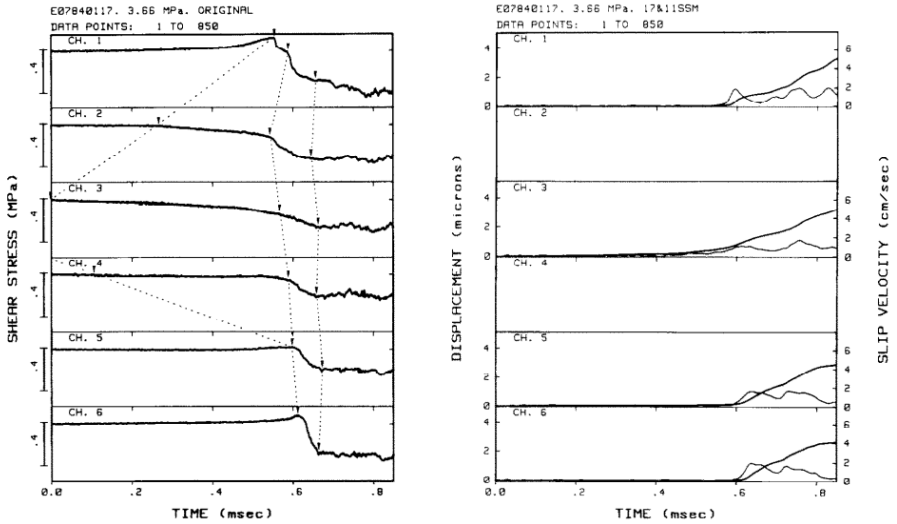

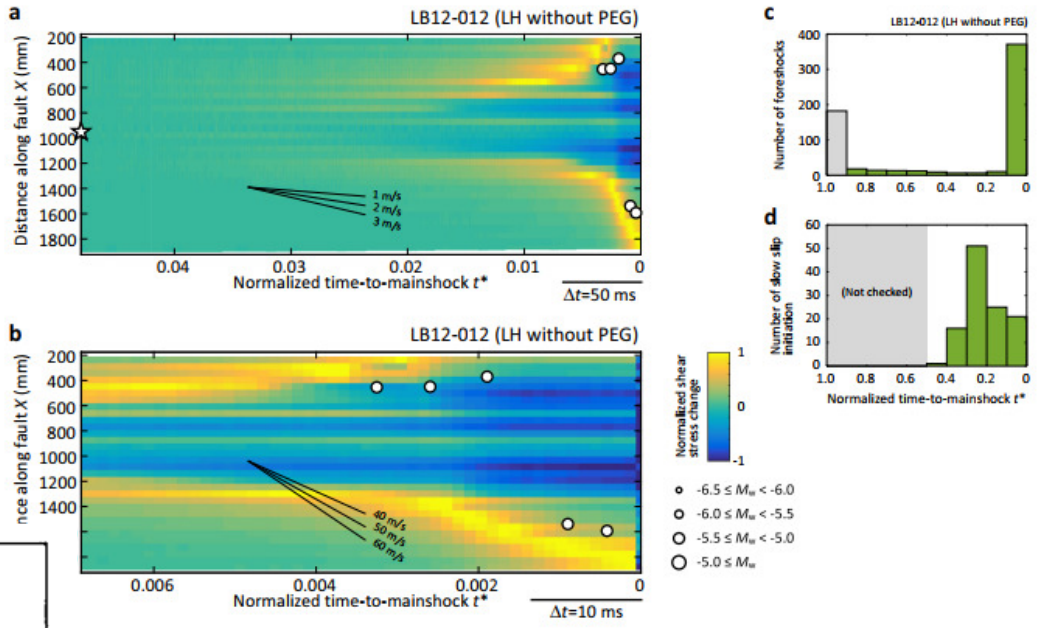

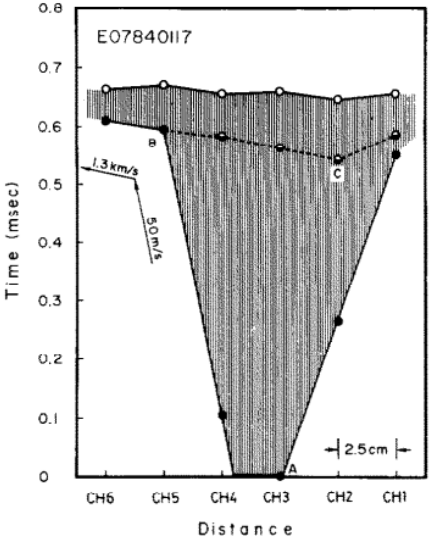

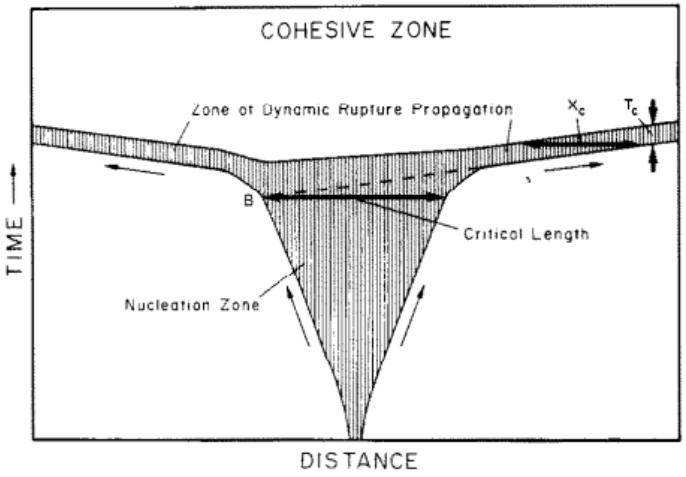

Ohnaka & Kuwahara (1990)

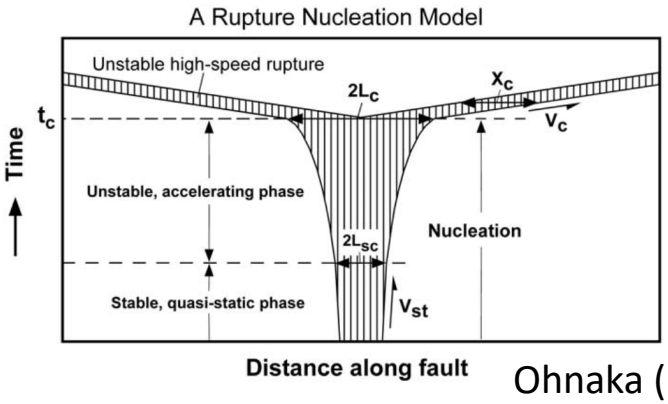

Ohnaka (2003)

Friction law inferred from seismological observation

Ide & Takeo (1997): 1995 Kobe earthquake

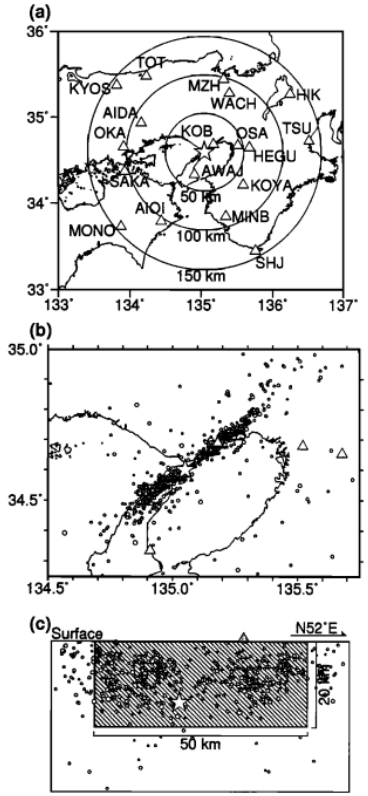

Figure 2. (a) Location map of strong-motion stations used in our analysis. The mainshock hypocenter and the assumed fault plane are shown by a star and a solid line, respectively. (b) Locations of aftershocks determined by Japanese University Group for Urgent Joint Observation of the 1995 Hyogo-ken Nanbu Earthquake [*Hirata et al.*, 1996]. The mainshock hypocenter is also represented by a star. Hatched rectangle represents the assumed fault plane. (c) Same as Figure 2b projected onto the assumed fault plane.

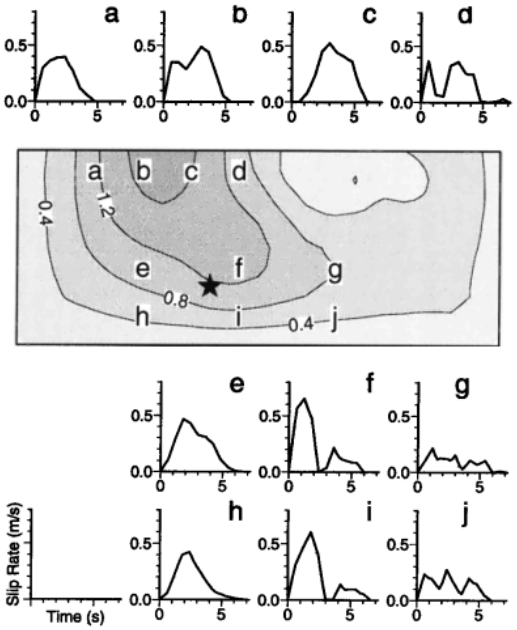

Figure 4. Total slip distribution of the Kobe earthquake and its source time functions at 10 selected points shown by a-j in the slip distribution. The source time functions show change of slip rate with 7.2 s time window after the arrival of an imaginary rupture front. Star represents the mainshock hypocenter.

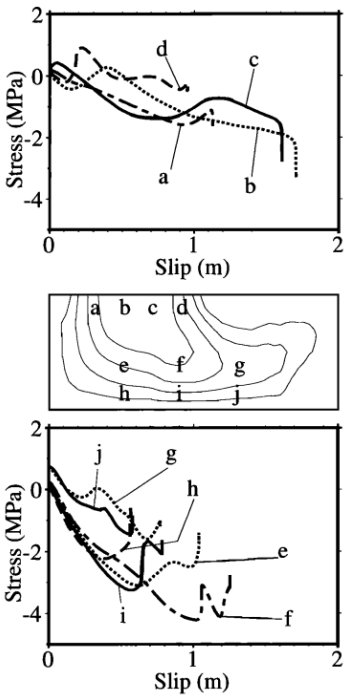

Figure 8. The constitutive relation between slip and stress on the fault plane. Each trace is the function calculated at the corresponding location in the middle figure of slip distribution.

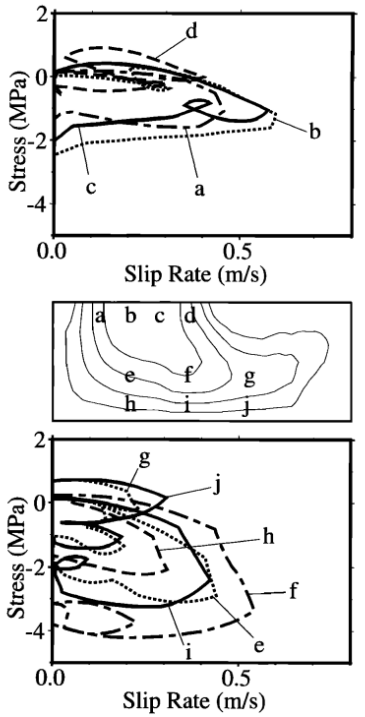

Figure 9. The relation between slip rate and stress. Each trace is the function calculated at the corresponding location in the middle figure of slip distribution.

Friction law inferred from seismological observation

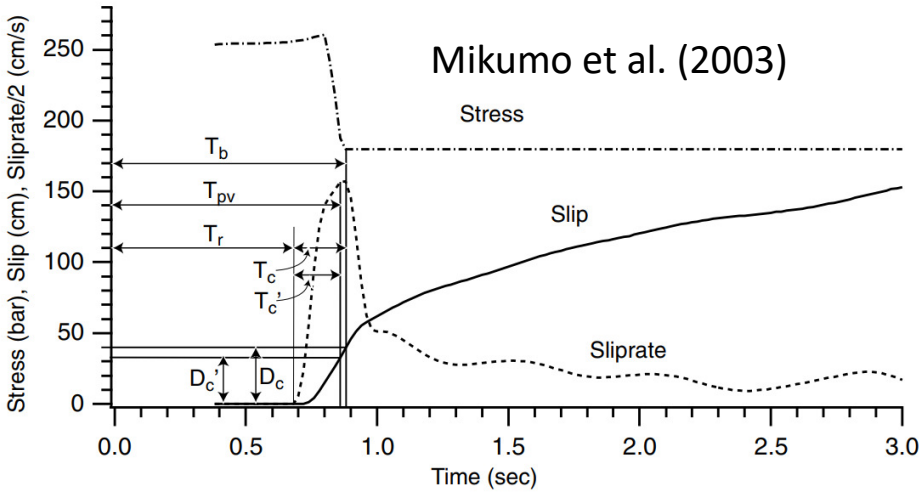

Figure 3. A typical behavior of the time history of shear stress, slip, and slip velocity on the fault. T_b, breakdown time of stress; T_{pv}, time of peak slip-velocity; D_c, slip at time T_b; D_c', slip at time T_{pv}.

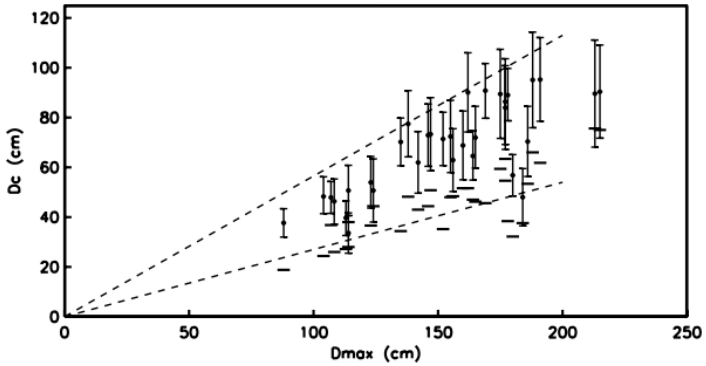

Figure 15. The estimated D_c values with their minimum resolvable limit (thick horizontal bars) and probable errors (thin vertical lines) plotted versus the local maximum slip on all subfaults. The two dashed lines depict the upper and lower ranges of data $D_c = 0.56\ D_{max}$ (upper) and $D_c = 0.27\ D_{max}$ (lower).

2000 Tottori earthquake

An aftershock of 2000 Tottori earthquake

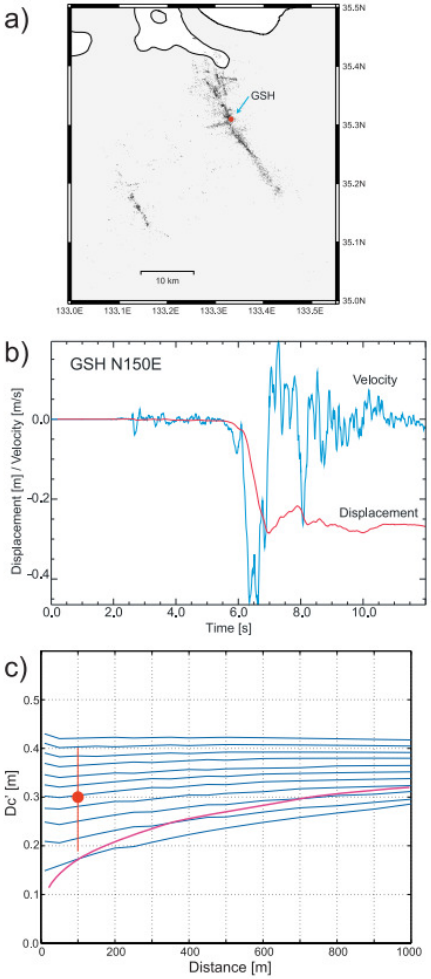

Fukyuama & Mikumo (2007)

2023 Türkiye (Turkey) earthquake

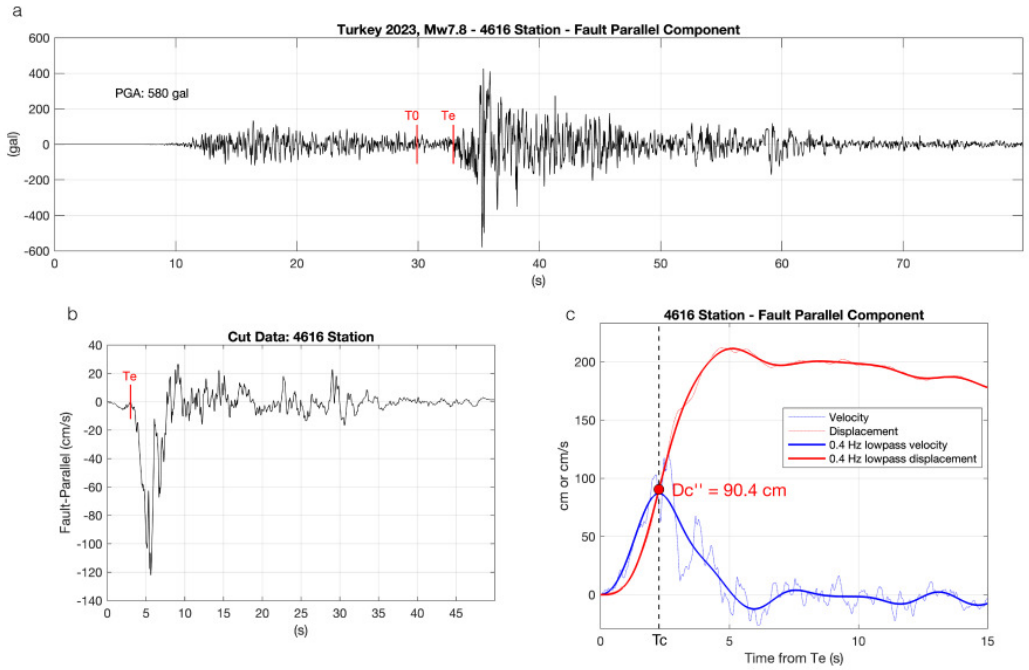

Figure 4 Processing of strong motion data at station 4616 for the estimation of fault cohesive zone parameters. (a) Raw fault-parallel (N30°E) acceleration record, where Te is the estimated arrival time of the main shock wave and T0 is the initial time for further analysis. (b) Velocity window starting at T0 after one integration using an automated baseline correction algorithm and 1 s tapering. Note that Te is clearly defined in the velocity waveform. (c) Velocity and displacement (double integration by the same method) seismograms starting at Te, low-pass filtered at 0.4 Hz and unfiltered. Proxies for the stress breakdown time, Tc, and the slip-weakening distance, D_c'', are given at the time of peak velocity (see text).

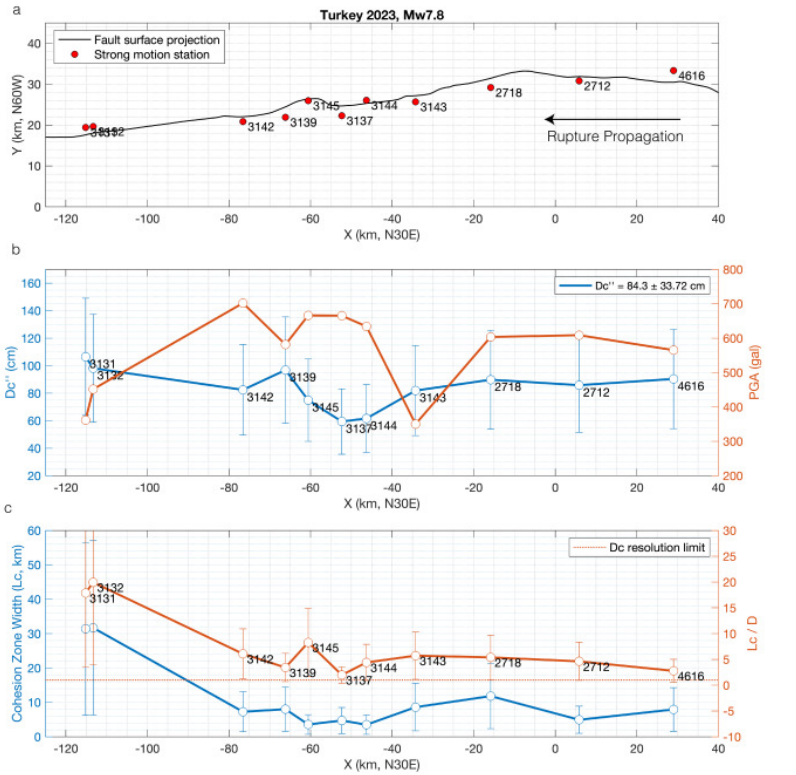

Figure 5 Estimates of dynamic source parameters from acceleration records within 3 km from the fault trace. (a) Fault surface projection and strong motion stations. (b) Proxy of the slip weakening distance, D_c'' (left axis, blue curve), and peak ground acceleration (geometric mean of horizontal components) (right axis, red curve). Note the anti-correlation between the two observables. (c) Width of the rupture front cohesive zone, Lc, assuming an average rupture velocity of 3.5 km/s (left axis, blue curve). Error bars contain 40% uncertainties on rupture velocity and stress breakdown times (see text). The slip-weakening distance, D_c, can only be reliably estimated for distances to the fault (D) shorter than Lc. The red curve (right axis) depicts the ratio Lc / D, so sites with values greater than 1 (red dotted line) are likely at a good resolution distance for D_c estimates. Note that all stations are above the resolution threshold.

Aochi & Cruz-Atienza (2025)

Critical crack (rupture nucleation) size (Lc)

Andrews (1976) and others

Displacement on crack of length $2L$ due to stress change from τ_0 to τ_f $\quad u = \frac{\tau_0 - \tau_f}{\mu}(L^2 - x^2)^{1/2}$ 2D solution

$$-\delta(E - W) = \delta\Pi$$

(discontinuity $\Delta u = 2u$)

Potential energy of system (strain energy – work done along boundary)

$$-\delta E = \frac{\tau_0 + \tau_f}{2}\int_{-L}^{+L} \Delta u\, dx = \frac{\pi}{2}\frac{1}{\mu}(\tau_0 + \tau_f)(\tau_0 - \tau_f)L^2$$

$$\delta W = -\tau_f \int_{-L}^{+L} \Delta u\, dx$$

$$-\delta(E - W) = \frac{\pi}{2}\frac{1}{\mu}(\tau_0 - \tau_f)^2 L^2$$

Under a hypothesis that the average stress did this work quasi-statically

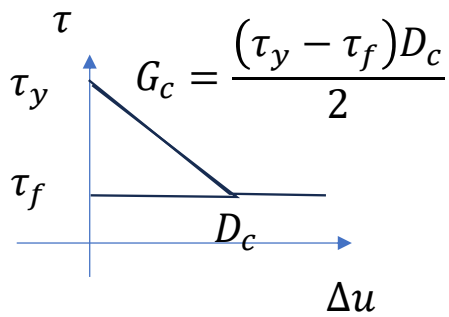

Energy for a crack extension of dL $\quad d(-\delta E - \delta\Pi) = \pi\frac{1}{\mu}(\tau_0 - \tau_f)^2 L\, dL$

This should be equivalent to the work done on the new part of the crack $\quad \delta\Pi = G_c(2dL)$

$$L_c = \frac{2}{\pi}\frac{\mu G_c}{(\tau_0 - \tau_f)^2} = \frac{\mu}{\pi}\frac{(\tau_y - \tau_f)D_c}{(\tau_0 - \tau_f)^2}$$

$D_c = 1\ \mu m \Rightarrow L_c \sim 20\ mm$

$D_c = 0.5\ m \Rightarrow L_c \sim 10\ km$

JOURNAL OF GEOPHYSICAL RESEARCH, VOL. 94, NO. B4, PAGES 4089–4104, APRIL 10, 1989

A Cohesive Zone Model for Dynamic Shear Faulting Based on Experimentally Inferred Constitutive Relation and Strong Motion Source Parameters

MITIYASU OHNAKA AND TERUO YAMASHITA

Earthquake Research Institute, University of Tokyo, Bunkyo-ku, Tokyo

To understand constitutive behavior near the rupture front during an earthquake source shear failure along a preexisting fault in terms of physics, local breakdown processes near the propagating tip of the slipping zone under mode II crack growth condition have been investigated experimentally and theoretically. A physically reasonable constitutive relation between cohesive stress τ and slip displacement D, $\tau = (\tau_i - \tau_d)[1 + \alpha \log(1 + \beta D)] \exp(-\eta D) + \tau_d$, is put forward to describe dynamic breakdown processes during earthquake source failure in quantitative terms. In the above equation, τ_i is the initial shear stress on the verge of slip, τ_d is the dynamic friction stress, and α, β, and η are constants. This relation is based on the constitutive features during slip failure instabilities revealed in the careful laboratory experiments. These experiments show that the shear stress first increases with ongoing slip during the dynamic breakdown process, the peak stress is attained at a very (usually negligibly) small but nonzero value of the slip displacement, and then the slip-weakening instability proceeds. The model leads to bounded slip acceleration and stresses at and near the dynamically propagating tip of the slipping zone along the fault in an elastic continuum. The dynamic behavior near the propagating tip of the slipping zone calculated from the theoretical model agrees with those observed during slip failure along the preexisting fault much larger than the cohesive zone. The model predicts that the maximum slip acceleration $\ddot{D}_{max}$ be related to the maximum slip velocity $\dot{D}_{max}$ and the critical displacement D_c by $\ddot{D}_{max} = k\dot{D}^2_{max}/D_c$, where k is a numerical parameter, taking a value ranging from 4.9 to 7.2 according to a value of τ_i/τ_p (τ_p being the peak shear stress) in the present model. The model further predicts that $\ddot{D}_{max}$ be expressed in terms of $\dot{D}_{max}$ and the cutoff frequency f^s_{max} of the power spectral density of the slip acceleration on the fault plane as $\ddot{D}_{max} = (3.6 \sim 4.4)\dot{D}_{max} f^s_{max}$ and that $\dot{D}_{max}$ in terms of D_c and f^s_{max} as $\dot{D}_{max} = (0.6 \sim 0.9)D_c f^s_{max}$. These theoretical relations agree well with the experimental observations and can explain interrelations between strong motion source parameters for earthquakes. The pulse width of slip acceleration on the fault plane is directly proportional to the time T_c required for the crack tip to break down, and f^s_{max} is inversely proportional to T_c.

$$f_{max} = 1/T_c$$

$$T_c = 0.53\pi^2 C(V)\frac{\mu}{\Delta\tau_b}\frac{D_c}{V}$$

Breakdown (cohesive) zone size (Xc)

$$\frac{D_c}{X_c} = k\frac{\Delta\tau_b}{\mu} \qquad k = \frac{\Gamma}{\pi^2 C(V)\xi}, \Gamma = \int_0^1 \frac{\sigma(Y)}{\sqrt{Y}}dY$$

$k \sim 3$, supposing $\frac{\Gamma}{\xi} = 3.3, V = 0.8V_s$

$$D_c = 1\ \mu m \quad \Rightarrow \quad X_c \sim 50\ mm$$

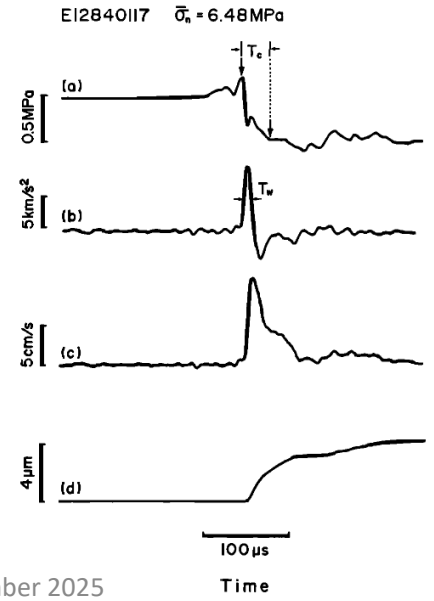

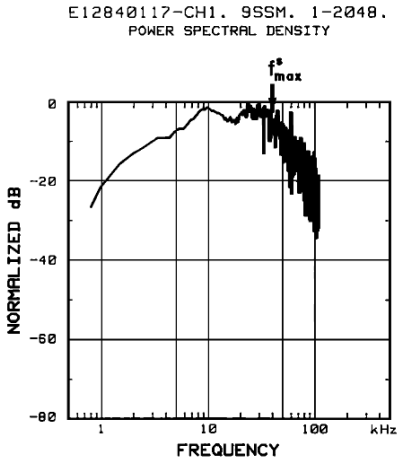

MAX. POWER SPECTRAL DENSITY = 9.9953E+015
FREQUENCY RESOLUTION = 4.8828E+02 Hz
FOLDOVER FREQUENCY = 5.0000E+05 Hz = POINT 1024

Fig. 7. An example of the power spectral density of a slip acceleration–time record. The upper limit of spectral band is denoted by f^s_{max}.

Numerical simulation of nucleation process

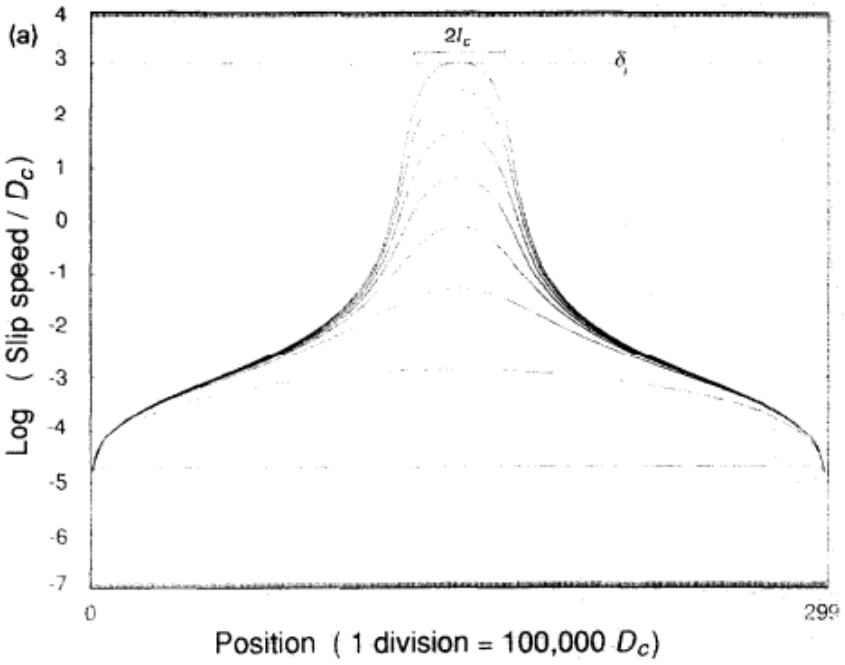

Dieterich (1992) with rate- and state-friction law

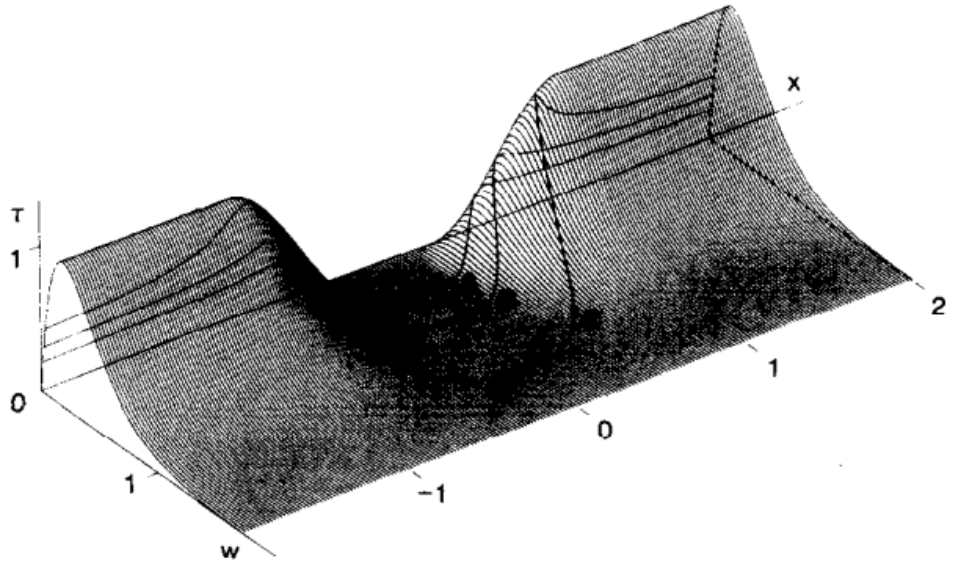

Matsu'ura et al. (1992) with slip-dependent friction law

Rate- and state-friction law

Ruina (1983) “Slip instability and stage variable friction laws”

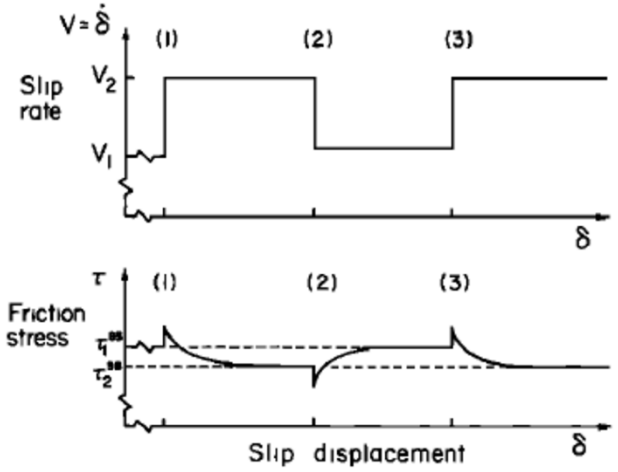

Fig. 1*b*. Idealized evolution of friction stress τ, at constant normal stress σ, when the slip rate $\dot{\delta} = V$ is changed. At location 1 the slip rate is suddenly increased from V_1 to V_2, τ jumps up from τ_1^{ss} and subsequently decays to τ_2^{ss}. At location 2, a sudden drop in slip rate back to V_1 causes a sudden drop in τ followed by a slow recovery to τ_1^{ss}. At location 3 the picture at location 1 is repeated.

$$\tau = \sigma[\mu_0 + \theta + A \ln (V/V_c)] \qquad (18a)$$

$$\dot{\theta} = (-V/d_c)[\theta + B \ln (V/V_c)] \qquad (18b)$$

Cocco and Bizzari (2002) “On the slip-weakening behavior of rate- and state dependent constitutive laws”

[1] We study the dynamic traction behavior within the cohesive zone during the propagation of earthquake ruptures adopting rate- and state-dependent constitutive relations. The resulting slip-weakening curve displays an equivalent slip-weakening distance (D_0^{eq}), which is different from the parameter L controlling the state variable evolution. The adopted constitutive parameters (a, b, L) control the slip-weakening behavior and the absorbed fracture energy. The dimension of the nucleation patch scales with L and not with D_0^{eq}. We propose a scaling relation between these two lengthscale parameters which prescribes that $D_0^{eq}/L \sim 15$. *INDEX TERMS:* 7209 Seismology: Earthquake

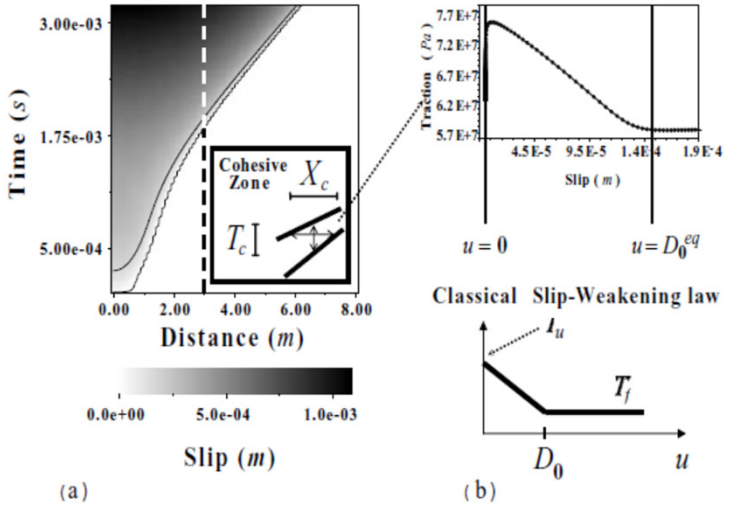

Stability analysis of friction

Scholtz (1990) “The mechanics of earthquakes and faulting” (1st ed.)

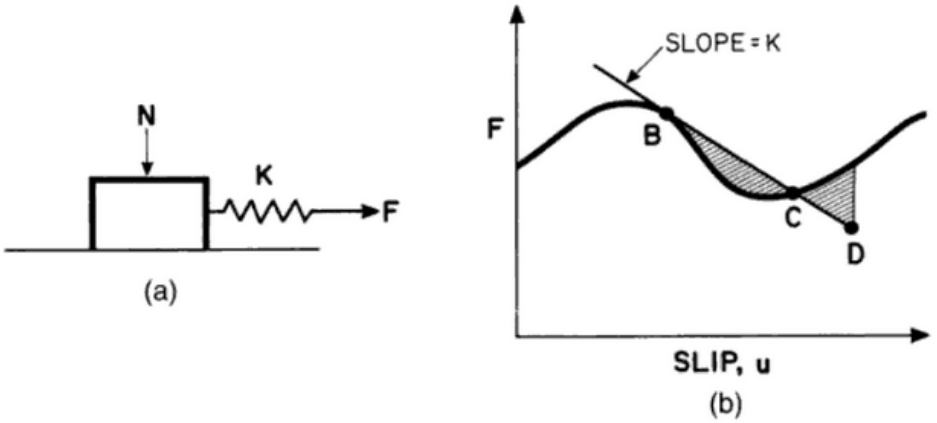

Fig. 2.16. Schematic diagram illustrating the origin of frictional instability: (a) a block-slider model; (b) a force–displacement diagram showing a hypothetical case in which the frictional resistance force falls with displacement at a rate faster than the system can respond.

Dieteric (1978), Ruina (1983)

Tse & Rice (1984) Crustal earthquake instability in relation to the depth variation of frictional sip properties.

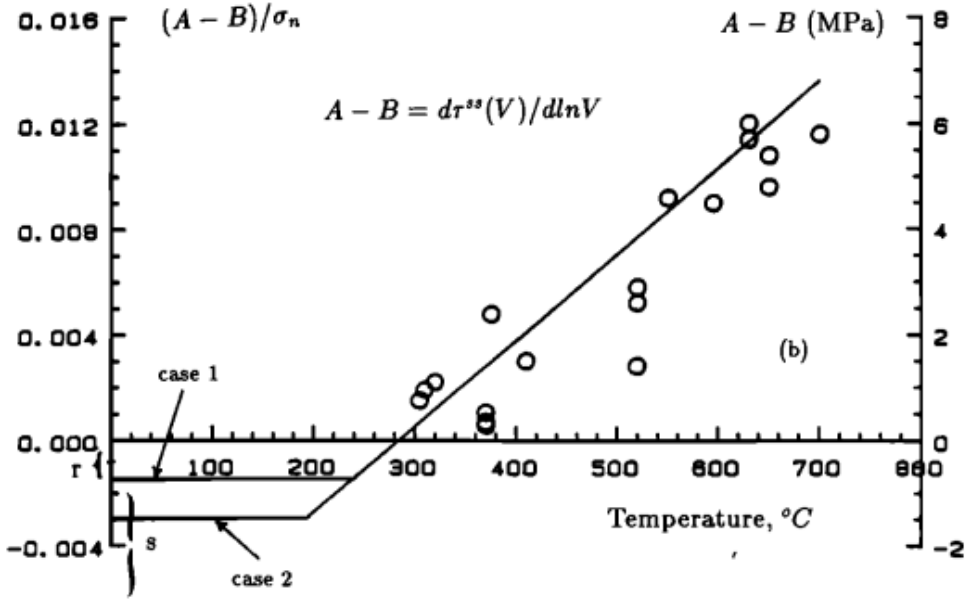

Further reading

- Thomas & Bhat (2002). Friction laws and numerical modeling of the seismic cycle, in *The seismic cycle: from observation to modeling*. Available on arxiv.org/pdf/2301.01605.